Q Controllable Antenna as a Potential Means for Wide-Area Sensing and Communication in Wireless Charging via Coupled Magnetic Resonances

Sousuke Nakamura, *Member, IEEE*, Masato Namiki, *Student Member, IEEE*, Yasuhiro Sugimoto, *Senior Member, IEEE*, and Hideki Hashimoto, *Fellow, IEEE*

***Abstract*—Recently, wireless charging via coupled magnetic resonances gains attention because it has a potential of efficient mid-range wireless charging. Here, functions such as sensing at the transmitter and wireless communication from the target are the essential elements to realize the standard wireless charging system. Currently, the sensing and communication protocol of hardware (i.e., high-frequency power source and antenna configuration) compatible with wireless charging is gaining attention in terms of cost and space reduction due to the use of common components in multiple functions. However, these protocols have the problem of narrow effective areas. Therefore, this paper presents a method for wide-area sensing and communication with slight modification of the configuration. The basic concept is to expand the effective area related to antenna *Q* factor by using the *Q* controllable antenna acting as though the *Q* factor increased. The underlying theory was described with electric circuit theory. The experimental results showed that the *Q* factor can be increased until the resonance collapses, and the increase of *Q* factor has the potential to widen the effective area of sensing and communication.**

***Index Terms*—Communication, coupled magnetic resonances, sensing, wide-area, wireless charging system.**

I. Introduction

In recent years, there have been various research works on wireless charging by magnetically coupled antennas [1]–[12]. Optimization of the antenna design, such as segmenting the transmitter antenna into several subsections in order to reduce the input voltage [1] and power losses [2], has been one of the major advances in the field. Moreover, wireless charging via coupled magnetic resonances has recently gained attention because it has a potential of efficient mid-range wireless charging [7]–[12]. This is due to the fact that it has a wider transmission range than electromagnetic induction charging [3]–[6] and ideally higher transmission efficiency in nonradiative manner than microwave [13] or laser charging [14]. Wireless charging via coupled magnetic resonances uses a pair of magnetically coupled antennas (i.e., coils) with additional capacitance, which makes the transmitter and the target to operate in the same resonant frequency. This addition of resonance effect enables power transmission over a longer distance than electromagnetic induction charging.

So far, the standard protocol of wireless charging system via magnetic coupling (e.g., coupled magnetic resonances, electromagnetic induction) [15]–[17], the so-called Qi standard, has been created by the "Wireless Power Consortium." The consortium was founded in 2009 by international companies. In this protocol, the wireless charging system works in two major phases: initialization and power transfer phase.

The initialization phase is composed of subphases: selection phase, ping phase, and identification and configuration phase. First, in the selection phase, the transmitter detects the target. Then, in the ping phase, the transmitter checks if the target has demand for power transmission and is compatible with the standard protocol, through wireless communication from the target. Finally, in the identification and configuration phase, the transmitter decides to accept or refuse to power the target by referring to the magnetic coupling between the target and configuration parameters communicated from the target (e.g., maximum required power, circuit element values).

After the initialization, the system moves on to the power transfer phase. Here, the transmitting power is controlled to let the charging power reach the required power. To enable this, the difference between charging power and required power termed as "control error" is communicated from the target. Power transfer lasts until the terminating signal is communicated or the magnetic coupling between the target becomes weak. When the power transfer phase is terminated, the system goes back to the initialization phase.

Thus, functions such as sensing at the transmitter and wireless communication from the target are the essential elements in the system.

This paper deals with passive magnetoquasistatic sensing and ASK-type load modulation as the protocol of sensing and communication. These protocols are hardware compatible with wireless charging and, specifically, share the high-frequency power source and antenna configuration with the configuration of wireless charging. The use of common components in multiple functions offers advantages of cost and space reduction.

Manuscript received May 5, 2015; revised July 24, 2015, October 2, 2015, and December 9, 2015; accepted January 11, 2016. Date of publication February 26, 2016; date of current version September 16, 2016. Recommended for publication by Associate Editor S.-C. Tan.

The authors are with the Department of Electrical, Electronic, and Communication Engineering, Chuo University, Tokyo 112-8551, Japan (e-mail: nakamura@elect.chuo-u.ac.jp; a10.pdch@g.chuo-u.ac.jp; sugimoto@elect.chuo-u.ac.jp; hashimoto@elect.chuo-u.ac.jp).

Color versions of one or more of the figures in this paper are available online at http://ieeexplore.ieee.org.

Digital Object Identifier 10.1109/TPEL.2016.2535259

A. Passive Magnetoquasistatic Sensing as the Sensing Protocol

The passive magnetoquasistatic sensing is one of the hopeful Qi standard sensing protocols of hardware compatible with wireless charging via magnetic coupling [18]–[20].

The electromagnetic sensing based on a pair of antennas is classified into two types: passive [18]–[22] and active [18], [23]–[27]. The relevance of passive type, which integrates the measurement device into transmitter antenna side, is increasing because the structure in the target becomes simple and cost-effective. In response, the passive type of magnetoquasistatic sensing [18]–[20], a form of electromagnetic sensing composed of a pair of magnetically coupled antennas (i.e., coils), has been studied as a protocol of hardware compatible with wireless charging via magnetic coupling. The protocol estimates the coupling coefficient from the input impedance measured at the transmitter side. These sensing offers coupling coefficient (i.e., strength of magnetic coupling) itself or position information derived from positional dependence of the coupling coefficient. On the other hand, the concept of selecting the coils from the arrayed coils for power transmission based on the detected target location [4]–[6] has gained attention. Thus, combining these two approaches, a method using passive magnetoquasistatic sensing for electromagnetic induction charging, the so-called coil array method [15]–[17], has been proposed as the Qi standard. In this method, among the arrayed coils, a coil with sufficient coupling coefficient between the target coil is activated as the power transmitter. Recently, the coil array method has been extended for use in wireless charging via coupled magnetic resonances [12], which results in the expansion of effective range with the resonance effect.

B. ASK-Type Load Modulation as the Communication Protocol

The ASK-type load modulation (i.e., backscattering modulation) is the majority in Qi standard communication protocol of hardware compatible with wireless charging via magnetic coupling [15]–[17].

In the load modulation, input impedance modulated by the change of target load impedance is demodulated into the corresponding digital data. Load impedance can be changed in several different ways—resistive [28], [29], reactive [30], or a combination of the two. How the load is changed affects the magnitude and phase of the input impedance. It acts like the ASK and PSK when the change in the load is resistive and reactive, respectively. In case of electromagnetic induction charging, load modulation of ASK-type is major due to its simple structure, while PSK-type has a benefit that the continuous wireless charging is possible during the communication [15], [16]. In case of wireless charging via coupled magnetic resonances, ASK-type is highly suitable because the phase shifting in the PSK-type leads to the lack of resonance while the resonance is maintained in ASK-type. Here, it is preferable to conduct power transmission and communication independently due to the fact that the parallel transmission of energy and data is disabled when the transmitted digital signal is LOW. Therefore, the communication time should be reduced to ensure the time for power transmission.

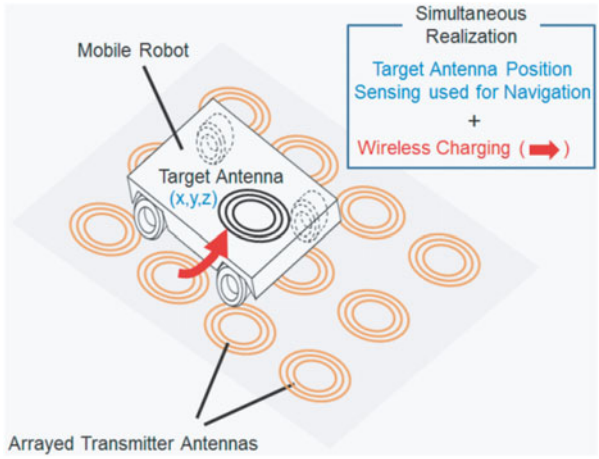

Fig. 1. Image of simultaneous realization of wireless charging and navigation for mobile robots.

C. Purpose of the Research

As mentioned above, the passive magnetoquasistatic sensing and ASK-type load modulation have advantages as the protocols in Qi standard wireless charging system via coupled magnetic resonances. However, there is still problem of insufficient sensing and communication range. Therefore, this paper presents a method for wide-area sensing and communication.

II. Demands for Wide-Area Sensing and Communication via Coupled Magnetic Resonances

Though the effective area of passive magnetoquasistatic sensing and ASK-type load modulation via coupled magnetic resonances is wider than that via electromagnetic induction due to the resonance effect, it is still insufficient. Widening the effective area of these sensing and communication protocols has potential benefits as follows.

Widening the effective area of the passive magnetoquasistatic sensing not only increases the convenience of the wireless charging, but also can be helpful in the localization [19], [20] for mobile robot navigation as shown in Fig. 1. The absolute position is estimated from the coupling coefficients between scattered transmitter antennas, and therefore, the widened effective area leads to reduction of the number of transmitter antennas.

One promising application is the automated guided vehicles (AGVs) in the factories. Here, wireless charging is required in clean factory automation of semiconductor industries due to its cleanness [3], and the localization using scattered permanent magnets [31] is known as the only method among others [32]–[34] to offer both open path navigation (i.e., the path is not fixed) and robustness to the environment (e.g., strength of the light, occlusion by other objects). The wireless charging using passive magnetoquasistatic sensing for sensing protocol can offer these characteristics with simple structures.

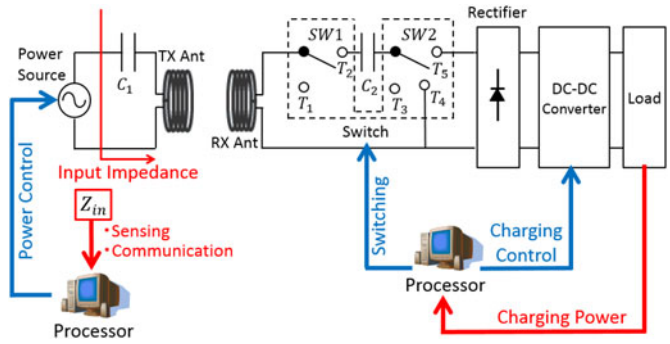

Fig. 2. Configuration of wireless charging system via coupled magnetic resonances.

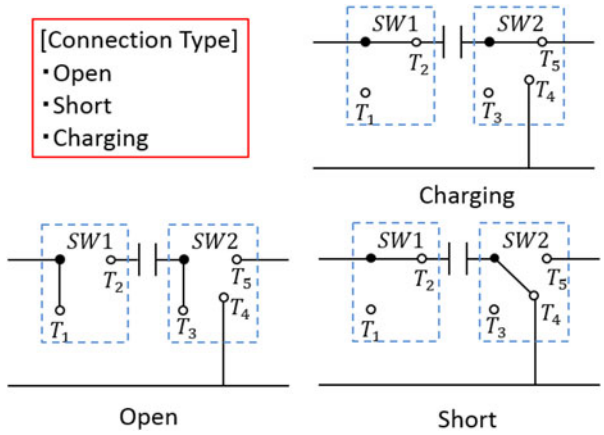

Fig. 3. Connection patterns of switches.

Widening the communication range of ASK-type load modulation not only has the direct advantage of enhancing the range itself, but the basic underlying technology has a potential to be diverted to other usage. For example, due to the increased sensitivity within the original communication range, the technology enables the use of multilevel modulation resulting in the reduction of the communication time. Reduction of the communication time, which leads to the extended time of power transmission, meets the requirements in ASK-type load modulation mentioned above.

III. Analysis of Effective Area in Conventional Sensing and Communication

A. System Configuration and Behavior

The configuration of the wireless charging system via coupled magnetic resonances is shown in Fig. 2. The passive magneto-quasistatic sensing and ASK-type load modulation are assumed for the sensing and communication protocols, respectively.

The system works in a combination of three functions: communication, sensing, and charging. The initialization phase works in a combination of communication and sensing functions, while the power transfer phase works in a combination of all functions. The high-frequency power source and antenna configuration are shared among the functions. For the antenna configuration, a compensation capacitor is used with the magnetic antenna (e.g., helical antenna, spiral antenna) to create the resonance conditions. The impedance measuring instrument is inserted in the transmitter side for the sensing and communication. The switches at the target side are used for switching the functions. Three types of connection of switches are expressed as Fig. 3.

In the communication function, the connections are switched between "open" and "short," which corresponds to the data bits. Thus, the connection of SW1 and SW2 are switched between T1·T3 and T2·T4, respectively. The switching of the switches is conducted simultaneously. The measured input impedance of "open" and "short" is demodulated into data bits. During the communication, the transmitting power is lowered to the level required for impedance measurement.

In the sensing function, the connections are set to "short." Thus, the SW1 and SW2 are connected to T2 and T4, respectively. The load acting as a variable resistor is disconnected to guarantee that the coupling coefficient is the only variable affecting the impedance. The coupling coefficient is estimated from measured input impedance and element values of the transmitter and target. The element values of the target are acquired beforehand through communication. During the sensing, the transmitting power is lowered to the level required for impedance measurement.

In the charging function, the connections are set to "charging." Thus, SW1 and SW2 are connected to T2 and T5, respectively, and the transmitting power is fed to the load through the magnetically coupled resonating antennas, rectifier, and dc–dc converter. The use of dc–dc converter enables controlling the charging voltage to certain value determined by the state of charge of the load. The transmitting power is controlled by referring to control error, terminating signal, and coupling coefficient. The control error and terminating signal are acquired through communication, while the coupling coefficient is acquired through sensing.

B. Analysis of Effective Area Based on Circuit Theory

The circuit diagram in case of sensing and communication is modeled as Fig. 4 by applying the electric circuit theory. Each antenna is expressed as a series-resonant circuit composed of series elements, R_i, L_i, and C_i $(i = 1, 2)$. L_m is the mutual inductance, which represents the magnetic coupling between antennas. The other circuit elements are as follows. $V_{\rm src}$ represents the voltage source and $Z_{\rm in}$ represents the measured input impedance as seen by the transmitter.

The transmitter and target antenna resonates at the same frequency f_0 to assure the coupled magnetic resonances occur. ω_0 represents the resonant angular velocity. The following discussion assumes that the coupled magnetic resonances occur, and (1) is satisfied:

$$\omega_0 L_i - \frac{1}{\omega_0 C_i} = 0 \quad (i = 1, 2), \quad \omega_0 = 2\pi f_0. \tag{1}$$

The coupling coefficient κ, a nondimensional form of the magnetic coupling strength, is expressed in (2) as the mutual

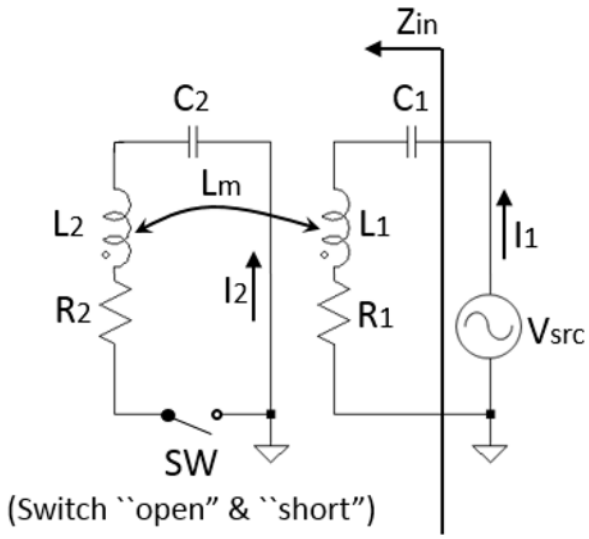

Fig. 4. Circuit diagram in case of sensing and communication.

inductance divided by the self-inductance:

$$\kappa = L_m/(L_1 L_2)^{1/2}. \tag{2}$$

The mutual inductance L_m is the only circuit element related to the mutual position of the antennas. Therefore, the coupling coefficient κ is also a physical quantity related to the mutual position of the antennas.

The input impedance $Z_{\rm in}$ of "short" and "open" are expressed as follows:

$$Z_{\rm in(short)} = \frac{\omega_0^2 L_m^2}{R_2} + R_1 = (\kappa^2 Q^2 + 1) R_1 \tag{3}$$

$$Z_{\rm in(open)} = R_1 \tag{4}$$

where

$$Q_i = \omega_0 L_i / R_i \ \ (i = 1, 2), \ \ Q = (Q_1 Q_2)^{1/2}. \tag{5}$$

The effective area of sensing and communication is discussed as follows.

The sensing function estimates the coupling coefficient from the measured input impedance and previously known fixed element values of the transmitter and target using the relation (3). The connections are kept "short" in the sensing function.

Here, the measurement error of the input impedance results in the estimation error of the coupling coefficient. The effective area of sensing is a set of mutual positions of antennas where the estimation error of coupling coefficient $\Delta\kappa$ is small. Among the physical quantity of (3), coupling coefficient is the quantity determined by the mutual position of antennas. Therefore, widening the effective area can be achieved by expanding a set of coupling coefficients where $\Delta\kappa$ is small. Condition to widen the effective area is derived by the following error analysis.

At first, the measurement error is described as follows. The network analysis method and RF *I–V* method are often used in the high-frequency impedance measurement [35]. The network analysis method calculates the input impedance from the measured reflection coefficient value Γ using (6), where Z_0 is the characteristic impedance of the measurement circuit. The error characteristics of reflection coefficient measurement are known to be approximated as (7) [36]. a and b are the positive constant values dependent on the dual-directional coupler used as reflection coefficient measurement device. Thus, the impedance measurement error $\Delta Z_{\rm in}$ can be derived from (6) and (7). On the other hand, the principle of the RF *I–V* method is based on the linear relationship of the voltage–current ratio to impedance, as given by Ohm's law. Thus, the impedance measurement error $\Delta Z_{\rm in}$ is constant, regardless of the $Z_{\rm in}$ value

$$\Gamma = \frac{Z_{\rm in} - Z_0}{Z_{\rm in} + Z_0} \tag{6}$$

$$\Delta\Gamma = a|\Gamma| + b \tag{7}$$

where

$$a > 0, \ \ b > 0.$$

Next, in order to discuss the condition to widen the effective area of sensing, $\Delta\kappa$ is formulated as (8) in network analysis method using (3), (6), and (7) under the condition of small coupling coefficient with sufficient antenna distance, and (9) in the RF *I–V* method using (3). It should be noted that the approximation $Z_{\rm in(short)} << Z_0$, which holds in the case of small coupling coefficient, is used in this derivation. Here, $S_{\rm sens}^{Z_{\rm in}}$ represents the sensitivity of input impedance to coupling coefficient.

1) In case of network analysis method

$$\Delta\kappa = \frac{\partial\kappa}{\partial Z_{\rm in(short)}} \frac{\partial Z_{\rm in(short)}}{\partial\Gamma} \Delta\Gamma \simeq \frac{1}{S_{\rm sens}^{Z_{\rm in}}} \frac{(b-a) Z_0}{2}. \tag{8}$$

2) In case of RF *I–V* method

$$\Delta\kappa = \frac{\partial\kappa}{\partial Z_{\rm in(short)}} \Delta Z_{\rm in(short)} = \frac{1}{S_{\rm sens}^{Z_{\rm in}}} \Delta Z_{\rm in(short)} \tag{9}$$

where

$$S_{\rm sens}^{Z_{\rm in}} \equiv \frac{\partial Z_{\rm in(short)}}{\partial\kappa} = 2 R_1 Q^2 \kappa. \tag{10}$$

The equations establish the well-known result that the sensing tends to fail as the coupling coefficient becomes small [18]–[20], because the smaller coupling coefficient leads to the decrease of $S_{\rm sens}^{Z_{\rm in}}$, which results in the increase of $\Delta\kappa$. However, the equations also show that this increase of $\Delta\kappa$ could be suppressed by the increase of Q factor. Thus, the increase of Q factor results in including the smaller coupling coefficients to the set of coupling coefficients within certain $\Delta\kappa$, which corresponds to widening the effective area.

The communication function demodulates the measured input impedance of "open" and "short" into data bits. The connections are switched between "open" and "short."

The effective area of communication is a set of mutual positions of antennas that enable demodulation of the measured

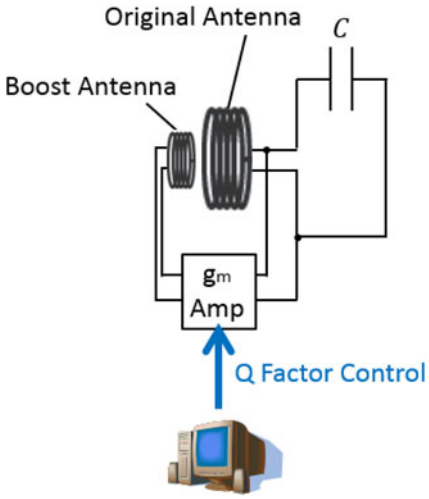

Fig. 5. Configuration of Q controllable antenna.

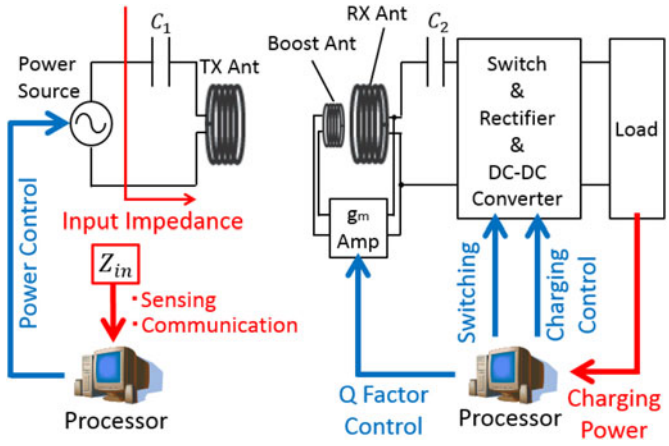

Fig. 6. Configuration of wireless charging system via coupled magnetic resonances with wide-area sensing and communication.

input impedance of "open" and "short" into data bits. This means that the effective area can be widened by expanding a set of coupling coefficients within the condition of difference in the input impedance of "open" (i.e., sensitivity of input impedance to data bits) and "short," represented as $S_{\rm com}^{Z_{\rm in}}$, larger than impedance measurement error $\Delta Z_{\rm in}$. $S_{\rm com}^{Z_{\rm in}}$ is formulated as follows using (3) and (4):

$$S_{\rm com}^{Z_{\rm in}} \equiv Z_{\rm in(short)} - Z_{\rm in(open)} = R_1 Q^2 \kappa^2. \tag{11}$$

The equation establishes the well-known result that the communication tends to fail as the coupling coefficient becomes small [28]–[29]. This is because $S_{\rm com}^{Z_{\rm in}}$ decrease as the coupling coefficient decreases and the communication finally fails when it is decreased to the level of the $\Delta Z_{\rm in}$. However, the equations also show that this decrease of $S_{\rm com}^{Z_{\rm in}}$ could be suppressed by the increase of Q factor. Thus, the increase of Q factor results in including the smaller coupling coefficients to the set of coupling coefficients within condition of $S_{\rm com}^{Z_{\rm in}}$ larger than $\Delta Z_{\rm in}$, which corresponds to widening the effective area.

Thus, it is concluded that the increase of Q factor, which can increase $S^{Z_{\rm in}}$ (i.e., $S_{\rm sens}^{Z_{\rm in}}$ and $S_{\rm com}^{Z_{\rm in}}$), enables widening of the effective area of both sensing and communication. In response, a novel antenna which enables the control of Q factor is introduced in the following section.

IV. Q Controllable Antenna

A. Basic Concept and Configuration of Q Controllable Antenna

Referring to the equation of Q factor expressed as (5), the control of Q factor can be possible by either controlling the self-inductance L or resistance R. However, these parameters are determined and fixed by the geometry and material of the manufactured antenna. Changing the perspective, instead of controlling the actual Q factor of the antenna, $S^{Z_{\rm in}}$ can also be increased with the antenna acting as though the Q factor increased. Thus, the antenna, which virtually acts as the Q factor increased, has been proposed.

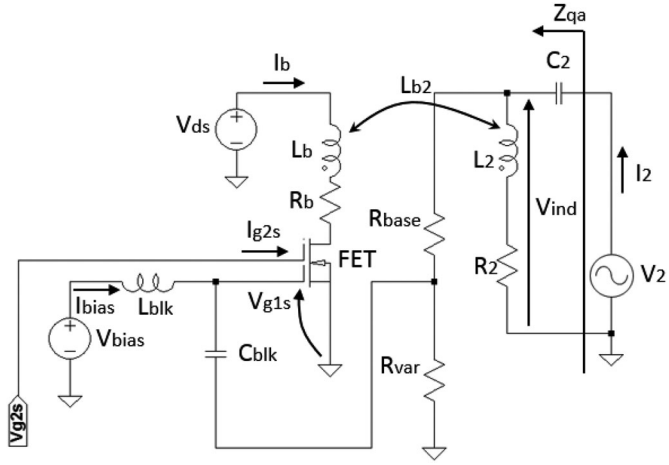

Fig. 7. Circuit diagram of Q controllable antenna.

The basic concept is to make the antenna act as if the resistance R is reduced by increasing the current flow caused by the source voltage. This is realized by feeding the energy to the original antenna from additionally attached antenna, termed boost antenna. As shown in Fig. 5, the Q controllable antenna has additional components of boost antenna and gm amplifier circuit compared to that of the standard antenna. The amount of energy fed from the boost antenna is regulated by the amplification level of gm amplifier circuit.

B. Behavior of the Q Controllable Antenna Based on Circuit Theory

As shown in Fig. 6, Q controllable antenna is applied to the target side in the wireless charging system via coupled magnetic resonances with wide-area sensing and communication. Here, the Q controllable antenna is configured by connecting the boost antenna and gm amplifier circuit to the original target antenna.

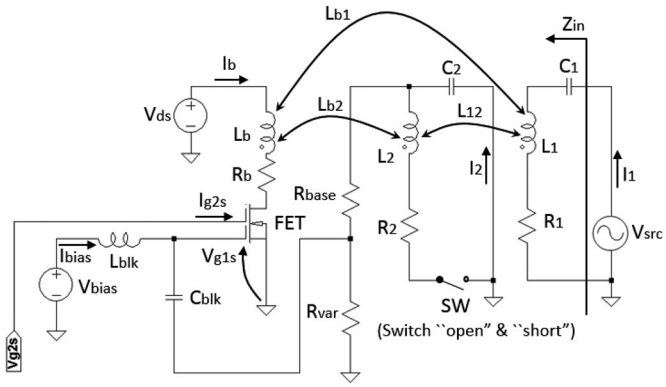

Fig. 8. Circuit diagram of wide-area sensing and communication.

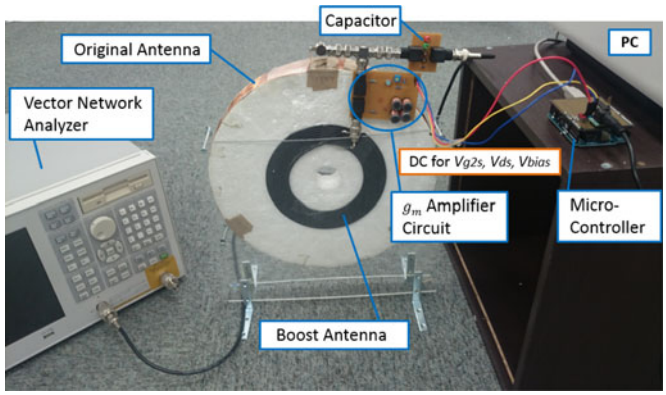

Fig. 9. Experimental setup of the Q controllable antenna.

Considering these facts, the behavior of Q controllable antenna itself is discussed as follows.

The circuit diagram of the Q controllable antenna is modeled as Fig. 7 by applying the electric circuit theory. The circuit is composed of elements expressing source voltage, antennas, and gm amplifier circuit. V_2 represents the source voltage of an original target antenna. This V_2 corresponds to the voltage induced from the transmitter antenna in the complete system shown in Fig. 6. I_2 represents the current flow in an original target antenna. Z_{qa} represents the equivalent impedance of the circuit defined as the value of V_2 divided by I_2. I_b represents the drain current and the ac and dc components of I_b are expressed as $I_{b\ (\mathrm{AC})}$ and $I_{b\ (\mathrm{DC})}$, respectively. Original target antenna is expressed as a series-resonant circuit composed of series elements, R_2, L_2, C_2. Boost antenna is an antenna without any compensation capacitor, expressed as a series element of R_b and L_b. The magnetic coupling between antennas is expressed as mutual inductance L_{b2}. The original target antenna is resonating at resonant angular velocity ω_0. The behavior of Q controllable antenna is described as follows.

The voltage between both ends of the coil inductance of the original target antenna, termed V_{ind}, is input to the gm amplifier circuit through voltage-dividing circuit. The gm amplifier circuit is the voltage-to-current converter composed of dual-gate FET operating in the saturation region. The dc voltage V_{bias} and V_{ds} are used as bias to ensure that the operating point is within the saturation region. The circuit converts the ac component of the voltage applied to gate 1, termed V_{g1s}, into $I_{b\ (\mathrm{AC})}$ in a same phase. The ratio of $I_{b\ (\mathrm{AC})}$ to V_{g1s}, termed amplification factor G_m, is controlled by the dc voltage V_{g2s} applied to gate 2. The choke coil L_{blk} and capacitor C_{blk} are used to block the ac and dc voltage, respectively. C_{g1s} represents the input capacitance of the gate 1 of the FET. The back electromotive force emerges in the original target antenna due to the magnetic field associated with the ac component of the drain current $I_{b\ (\mathrm{AC})}$. Since the back electromotive force becomes same phase with the source voltage, the circuit acts as though the external source is added to the source voltage V_2. Thus, the current flow I_2 increases even though the source voltage V_2 is constant, and consequently, the circuit acts as if the resistance R_2 reduced. These behaviors are expressed in following equations.

TABLE I
DESIGN PARAMETERS OF THE Q CONTROLLABLE ANTENNA

Parameter	Value	Unit
coil turns of helical target antenna	12	turn
coil pitch of helical target antenna	0.003	m
diameter of helical target antenna	0.3	m
coil turns of spiral boost antenna	9	turn
coil pitch of spiral boost antenna	0.0018	m
inner diameter of spiral boost antenna	0.096	m
outer diameter of spiral boost antenna	0.154	m
diameter of the wire used for antenna	0.001	m

$I_{b\ (\mathrm{AC})}$ is expressed as (12) using V_{g1s} and G_m, while V_{g1s} is determined by the voltage-dividing circuit as shown in (13). It should be noted that the inductive voltage by electromagnetic induction from original target antenna does not affect $I_{b\ (\mathrm{AC})}$ because the FET is operated in the saturation region

$$I_{b\ (\mathrm{AC})} = G_m V_{g1s} \tag{12}$$

$$V_{g1s} = \frac{R_{\mathrm{var}}}{R_{\mathrm{base}} + R_{\mathrm{var}}} V_{\mathrm{ind}}. \tag{13}$$

Substituting (13) into (12), $I_{b\ (\mathrm{AC})}$ is expressed as follows:

$$I_{b\ (\mathrm{AC})} = \frac{R_{\mathrm{var}} G_m}{R_{\mathrm{base}} + R_{\mathrm{var}}} V_{\mathrm{ind}}. \tag{14}$$

The application of Kirchhoff's voltage law around the original target antenna gives following equation:

$$\begin{aligned} V_2 &= R_2 I_2 + j\omega_0 L_{b2} I_{b\ (\mathrm{AC})} \\ &= R_2 I_2 + j\omega_0 L_{b2} g_m V_{\mathrm{ind}} \\ &= R_2 I_2 + j\omega_0 L_{b2} g_m (R_2 + j\omega_0 L_2) I_2 \end{aligned} \tag{15}$$

where

$$g_m = \frac{R_{\mathrm{var}} G_m}{R_{\mathrm{base}} + R_{\mathrm{var}}} \quad , \quad V_{\mathrm{ind}} = (R_2 + j\omega_0 L_2) I_2. \tag{16}$$

Thus, in case the Q factor of the original target antenna is high enough and condition (17) is satisfied

$$\alpha := \frac{R_2}{\omega_0 L_2} = \frac{1}{Q_2} \simeq 0 \tag{17}$$

TABLE II
CIRCUIT ELEMENT VALUES OF THE Q CONTROLLABLE ANTENNA

Parameter	Value	Unit
frequency f_0	1.0	MHz
resistance of target antenna R_2	3.510	Ω
inductance of target antenna L_2	85.97	μH
capacitance of target antenna C_2	292.74	pF
resistance of boost antenna R_b	2.275	Ω
inductance of boost antenna L_b	14.76	μH
mutual inductance between antennas L_{b2}	6.537	μH
inductance of AC blocking choke coil L_{blk}	1000	mH
capacitance of DC blocking capacitor C_{blk}	100	pF
capacitance of the gate 1 in FET C_{g1s}	0.967	pF
base resistance of voltage-dividing circuit $R_{\rm base}$	4.7	MΩ
regulation resistance of voltage-dividing circuit $R_{\rm var}$	43.4	kΩ
gate voltage for operation in saturation $V_{\rm bias}$	1.0	V
drain source voltage for operation in saturation $V_{\rm ds}$	12	V
incident power from the source $P_{\rm fwd}$	−25	dBm

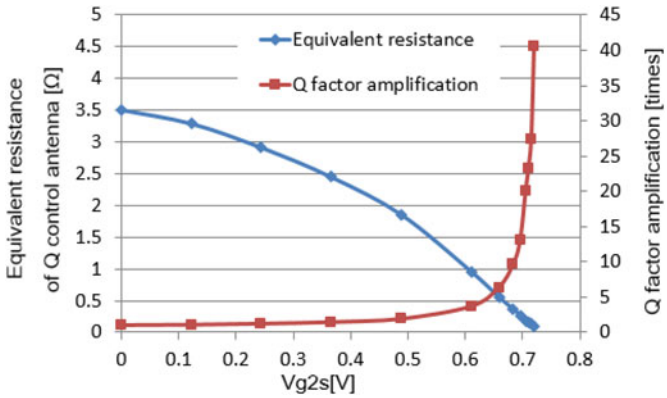

Fig. 10. Equivalent resistance $\mathrm{Re}(Z_{qa})$ and Q factor amplification versus control voltage V_{g2s}.

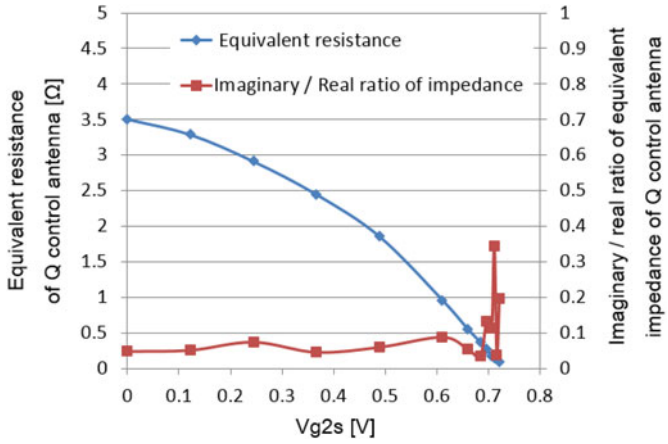

Fig. 11. Equivalent resistance $\mathrm{Re}(Z_{qa})$ and ratio of imaginary part $\mathrm{Im}(Z_{qa})$ to real part $\mathrm{Re}(Z_{qa})$ versus control voltage V_{g2s}.

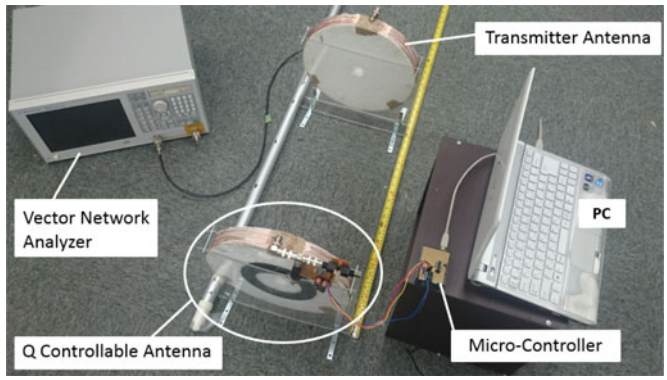

Fig. 12. Experimental setup of wide-area sensing and communication configuration

the equivalent impedance of the circuit Z_{qa} is approximated as follows:

$$Z_{qa} = \frac{V_2}{I_2} \simeq R_2 - g_m \omega_0^2 L_{b2} L_2. \quad (18)$$

Consequently, the equivalent impedance and the Q factor are changed as follows:

$$R_2 \longmapsto R_2 - g_m \omega_0^2 L_{b2} L_2 \quad (19)$$

$$Q_2 \longmapsto \frac{R_2}{R_2 - g_m \omega_0^2 L_{b2} L_2} Q_2. \quad (20)$$

C. Handling of the Q Controllable Antenna in the Charging Function

As mentioned above, even if the Q controllable antenna acts as though the Q factor increased, the Q factor of the original antenna is unchanged. This leads to the fact that the transmission efficiency, which is the ratio of power injected to transmitter antenna to transferred power to the target load originating from the transmitter antenna (excluding that originating from the power injected to Q controllable antenna), is identical to the case using original antenna. Therefore, the Q control function is turned OFF (control voltage V_{g2s} is set to 0 [V]) in the charging function in order to avoid the meaningless power consumption at the target side, .

Thus, in case of using Q controllable antenna instead of the original antenna, the power transmission ability is kept, while effective range in the sensing and communication becomes wider.

TABLE III
DESIGN PARAMETERS OF THE ANTENNAS IN CONFIGURATION OF WIDE-AREA SENSING AND COMMUNICATION

Parameter	Value	Unit
coil turns of helical transmitter antenna	12	turn
coil pitch of helical transmitter antenna	0.003	m
diameter of helical transmitter antenna	0.3	m
coil turns of helical target antenna	12	turn
coil pitch of helical target antenna	0.003	m
diameter of helical target antenna	0.3	m
coil turns of spiral boost antenna	9	turn
coil pitch of spiral boost antenna	0.0018	m
inner diameter of spiral boost antenna	0.096	m
outer diameter of spiral boost antenna	0.154	m
diameter of the wire used for antenna	0.001	m

TABLE IV
CIRCUIT ELEMENT VALUES OF THE CONFIGURATION OF WIDE-AREA SENSING AND COMMUNICATION

Parameter	Value	Unit
frequency f_0	1.0	MHz
resistance of transmitter antenna R_1	2.716	Ω
inductance of transmitter antenna L_1	86.529	μH
capacitance of transmitter antenna C_1	294.62	pF
resistance of target antenna R_2	3.510	Ω
inductance of target antenna L_2	85.97	μH
capacitance of target antenna C_2	292.74	pF
resistance of boost antenna R_b	2.275	Ω
inductance of boost antenna L_b	14.76	μH
mutual inductance between target and boost L_{b2}	6.537	μH
inductance of ac blocking choke coil L_{blk}	1000	mH
capacitance of dc blocking capacitor C_{blk}	100	pF
capacitance of the gate 1 in FET C_{g1s}	0.967	pF
base resistance of voltage-dividing circuit $R_{\rm base}$	4.7	MΩ
regulation resistance of voltage-dividing circuit $R_{\rm var}$	43.4	kΩ
gate voltage for operation in saturation $V_{\rm bias}$	1.0	V
drain source voltage for operation in saturation V_{ds}	12	V
incident power from the source P_{fwd}	−25	dBm

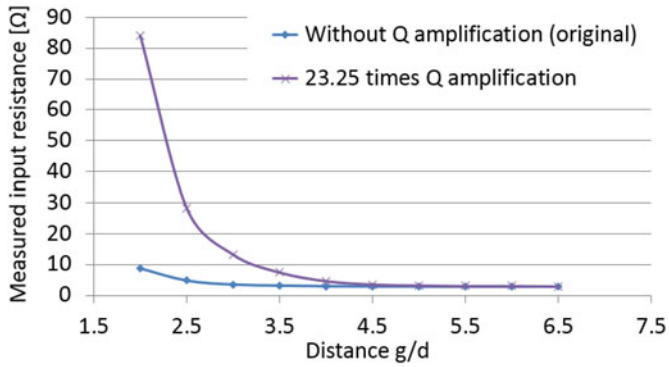

Fig. 13. Input resistance $\mathrm{Re}(Z_{\rm in(short)})$ versus normalized antenna distance g/d, in case of Q factor amplification of 23.25 times and no amplification.

V. CONFIGURATION AND BEHAVIOR OF WIDE-AREA SENSING AND COMMUNICATION

The circuit diagram of the sensing and communication configuration shown in Fig. 6 is modeled as Fig. 8 by applying the electric circuit theory. The transmitter and original target antenna is expressed as a series-resonant circuit composed of series elements, R_i, L_i, and C_i $(i = 1, 2)$. Boost antenna is expressed as a series element of R_b and L_b. The mutual inductances between antennas are expressed as L_{12}, L_{b1}, and L_{b2}. The circuit elements of gm amplifier circuit are same as the case of Fig. 7. I_1, I_2, and I_b represent the current flow in transmitter, original target, and boost antenna, respectively. The ac and dc component of I_b are expressed as $I_{b\ (\rm AC)}$ and $I_{b\ (\rm DC)}$, respectively. The $V_{\rm src}$ represents the source voltage, and $Z_{\rm in}$ represents the input impedance. The transmitter and original target antenna resonate at resonant angular velocity ω_0 to assure the magnetic resonance coupling to happen. The behavior in case the connections are set to "short" is analyzed from the following circuit

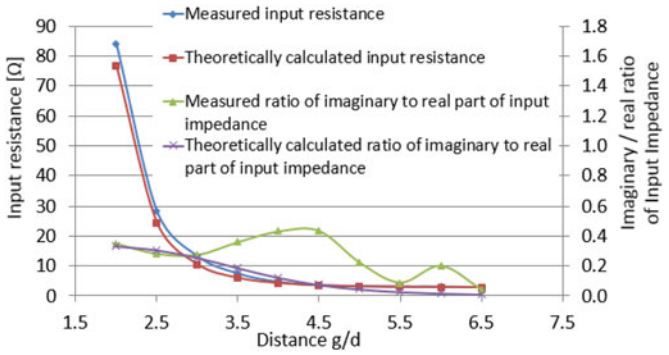

Fig. 14. Measured and theoretically calculated input resistance $\mathrm{Re}(Z_{\rm in(short)})$, and ratio of imaginary part $\mathrm{Im}(Z_{\rm in(short)})$ to real part $\mathrm{Re}(Z_{\rm in(short)})$ versus normalized antenna distance g/d, in case of Q factor amplification of 23.25 times.

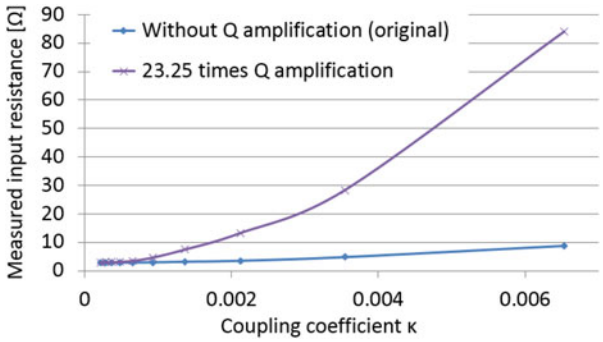

Fig. 15. Input resistance $\mathrm{Re}(Z_{\rm in(short)})$ versus coupling coefficient κ, in case of Q factor amplification of 23.25 times and no amplification.

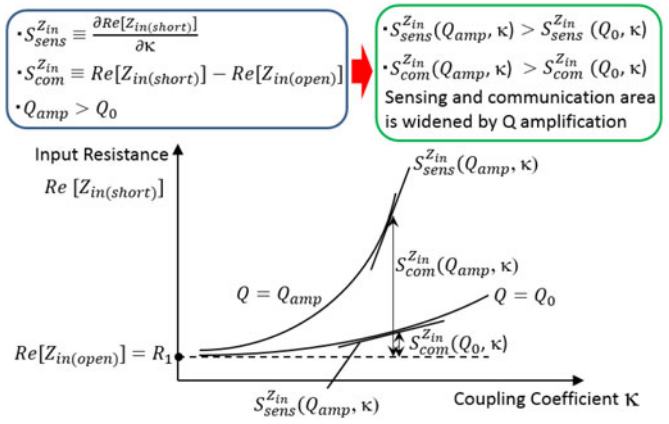

Fig. 16. Conceptual image of sensitivity of input impedance $S^{Z_{\rm in}}$ increasing as the Q factor increases from Q_0 to $Q_{\rm amp}$.

equations (21)–(23) of each antenna:

$$V_{\rm src} = R_1 I_1 + j\omega_0 L_{12} I_2 + j\omega_0 L_{b1} I_{b\ (\rm AC)} \quad (21)$$

$$0 = j\omega_0 L_{12} I_1 + R_2 I_2 + j\omega_0 L_{b2} I_{b\ (\rm AC)} \quad (22)$$

$$I_{b\ (\rm AC)} = g_m (R_2 + j\omega_0 L_2) I_2. \quad (23)$$

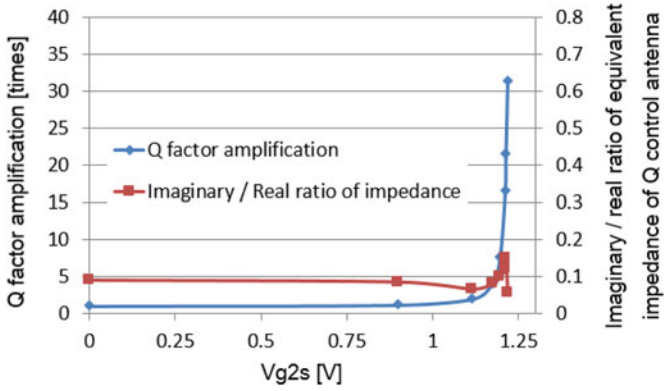

Fig. 17. Q factor amplification and ratio of imaginary part $\mathrm{Im}(Z_{\mathrm{in(short)}})$ to real part $\mathrm{Re}(Z_{\mathrm{in(short)}})$ versus control voltage V_{g2s} (the case of V_{ds}= 1.5 V).

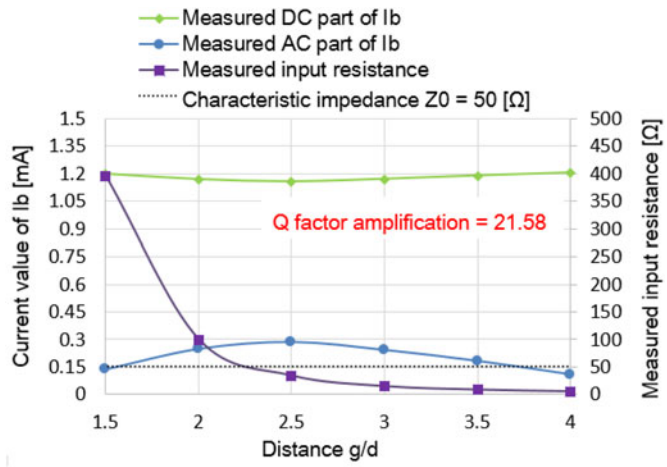

Fig. 18. AC/DC component of I_b and input resistance $\mathrm{Re}(Z_{\mathrm{in(short)}})$ versus normalized antenna distance g/d, in case of Q factor amplification of 21.58 times.

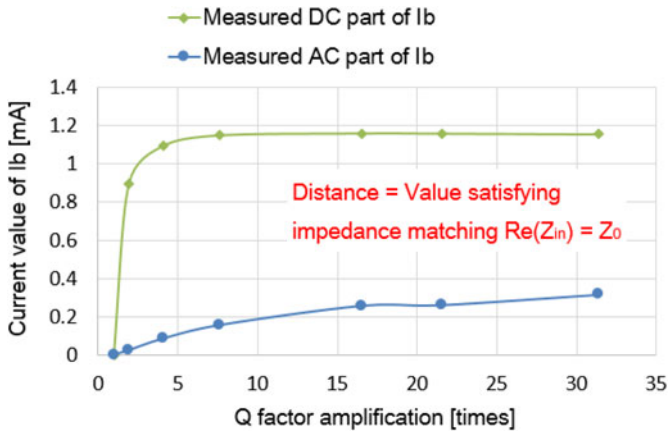

Fig. 19. AC/DC component of I_b versus Q factor amplification, in case of impedance matching distance.

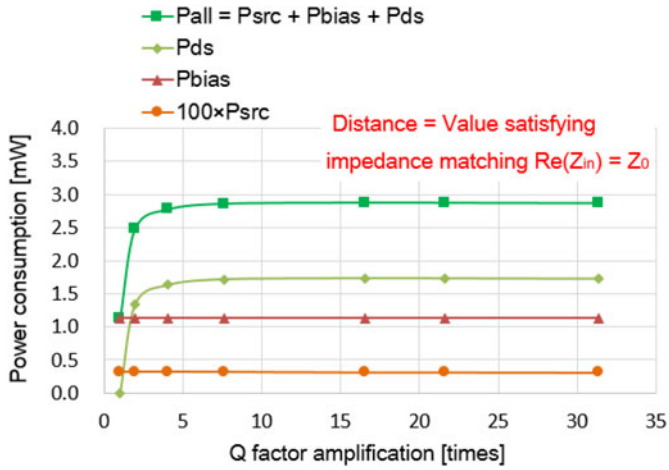

Fig. 20. Power consumption versus Q factor amplification, in case of impedance matching distance.

Thus, $Z_{\mathrm{in(short)}}$, the input impedance in case the connections are set to "short," is expressed as follows:

$$Z_{\mathrm{in(short)}} = \frac{V_{\mathrm{src}}}{I_1} = \frac{\omega_0^2 L_{12}^2 + g_m \omega_0^2 L_{12} L_{b1}(R_2 + j\omega_0 L_2)}{R_2 + j g_m \omega_0 L_{b2}(R_2 + j\omega_0 L_2)} + R_1. \tag{24}$$

In case conditions (25)–(27) are satisfied

$$\alpha := \frac{R_2}{\omega_0 L_2} = \frac{1}{Q_2} \simeq 0 \tag{25}$$

$$\beta := \frac{g_m \omega_0 L_{b1} L_2}{L_{12}} \simeq 0 \tag{26}$$

$$\gamma := \frac{L_{b1} L_2}{Q^2 L_{b2} L_{12}} \simeq 0 \tag{27}$$

the input impedance is approximated as

$$Z_{\mathrm{in(short)}} \simeq \frac{\omega_0^2 L_{12}^2}{R_2 - g_m \omega_0^2 L_{b2} L_2} + R_1. \tag{28}$$

If condition (27) is not satisfied, the distance between antennas effects the equivalent resistance of the Q controllable antenna. This condition could be satisfied by designing the Q factor of the antenna as high as possible.

Compared with the input impedance in the conventional configuration expressed as (3), the target resistance successfully became equivalent to that derived in (18). It should be noted that the input impedance in case the connections are set to "open" does not change from that in (4).

VI. Experiment

A. Impedance Characteristics of Q Controllable Antenna

The Q controllable antenna shown in Fig. 9 was developed. The corresponding circuit diagram is shown in Fig. 7. Toshiba 3SK293, the on-chip dual-gate FET usable up to frequency of UHF band, is selected for gm amplifier circuit. The original target antenna is structured as helical antenna with series compensation capacitor. The boost antenna is designed as relatively small spiral antenna which can be embedded in the target antenna so as to simplify the structure. The Q factor is controlled

TABLE V
SPECIFICATION OF COMMON DEVICES FOR POSITION SENSING AND COMMUNICATION

Method	Range	Position Estimation Error	Power Consumption	Combination use with Communication
LRF [38] (UBG-04LX-F01)	4 m	less than 0.04 m	8.4 W	No
Wi-Fi [39]	20 m	less than 3 m	50 mW	Yes
Zigbee [40]	5 m	less than 0.25 m	160 mW	Yes
UWB [41] (Decawave)	wider than 20 m	about 0.1 m	200 mW	Yes
Bluetooth [42]	10 m	less than 1 m	100 mW	Yes
Passive RFID [43]	2 m	less than 0.055 m	1 W	Yes
Polhemus Sensor [44] (FASTRAK)	0.76 m	7.6-mm RMS	15 W	No

by dc voltage V_{g2s} applied to gate 2 through microcontroller. The dc voltages $V_{\rm bias}$ and V_{ds} are set to ensure that the operating point of FET is within the saturation region. Design parameters of the antenna and circuit element values are shown in Tables I and II , respectively.

In the experiment, the equivalent impedance of the circuit Z_{qa} is measured for various V_{g2s} values. The impedance is measured by Agilent Technologies vector network analyzer (VNA) E-5061A. The impedance measurement of VNA is based on network analysis method. Fig. 10 shows that the equivalent resistance $\mathrm{Re}(Z_{qa})$ drops and the Q factor increases as the V_{g2s} increases. Moreover, Fig. 11 shows that the imaginary part of the impedance $\mathrm{Im}(Z_{qa})$ is suppressed compared to real part $\mathrm{Re}(Z_{qa})$ and the resonance is maintained. However, the resonance tends to collapse as the V_{g2s} increases because $\mathrm{Re}(Z_{qa})$ drops, while $\mathrm{Im}(Z_{qa})$ remains constant. Therefore, $\mathrm{Im}(Z_{qa})$ should be tuned to zero to avoid the resonance to collapse. Thus, it is concluded that the Q factor can be amplified until the resonance collapses.

B. Impedance Characteristics of Wide-Area Sensing and Communication Functions

The setup shown in Fig. 12was developed. The corresponding circuit diagram is shown in Fig. 8. The Q controllable antenna in this setup corresponds to that mentioned above. The transmitter antenna is structured as helical antenna with series compensation capacitor. Design parameters of the antenna and circuit element values are shown in Tables III and IV, respectively.

In the experiment, $Z_{\rm in(short)}$ is measured by changing the distance between antennas located in front of each other, for Q factor amplification of 23.25 times (V_{g2s}= 0.710 V) and no amplification (V_{g2s}= 0 V).

Fig. 13 shows that the input resistance $\mathrm{Re}(Z_{\rm in(short)})$ in case of Q factor amplification of 23.25 times is much higher than no amplification. The normalized distance g/d (where g is the actual distance and d is the antenna diameter) enables scale-free discussion independent of the antenna size. Fig. 14 shows that, in case of Q factor amplification of 23.25 times, the measured and theoretically calculated input resistance matches well, while the resonance is maintained to some extent.

Here, (28) assuming the complete resonance condition was not chosen for the calculation of theoretical value because the resonance tends to collapse (i.e., imaginary part of the impedance $\mathrm{Im}(Z_{qa})$ becomes nonnegligible) when the V_{g2s} increases. Instead, the calculation by (31) has been adopted using the measured equivalent impedance of the Q controllable antenna expressed as $Z_{qa(V_{g2s})}$. Here, (31) is derived as follows. Equation (21) is approximated to (29) by neglecting the comparatively small $j\omega_0 L_{b1} I_{b\ (\rm AC)}$ under (22), (23), (25), and (26). Equations (22) and (23) are replaced to (30) by applying the measured $Z_{qa(V_{g2s})}$ instead of the inaccurate value derived by electric circuit theory. As a consequence, (31) is derived from (29) and (30). Thus, the theoretical value is calculated from (31) by substituting the circuit element values in Table IV, premeasured equivalent impedance $Z_{qa(V_{g2s})}$, and mutual inductance L_{12} derived from the Neumann formula [37]:

$$V_{\rm src} = R_1 I_1 + j\omega_0 L_{12} I_2 \tag{29}$$

$$-j\omega_0 L_{12} I_1 = V_2 = Z_{qa(V_{g2s})} I_2 \tag{30}$$

$$Z_{\rm in(short)} = \frac{V_{\rm src}}{I_1} \simeq j\omega_0 L_{12}\frac{I_2}{I_1} + R_1 = \frac{\omega_0^2 L_{12}^2}{Z_{qa(V_{g2s})}} + R_1. \tag{31}$$

For further analysis, Fig. 15 shows the input resistance $\mathrm{Re}(Z_{\rm in(short)})$ versus coupling coefficient κ. The coupling coefficients correspond to each antenna distance mentioned above. $Z_{\rm in(short)}$ and $Z_{\rm in(open)}$ of (10) and (11) correspond to $\mathrm{Re}(Z_{\rm in(short)})$ discussed here and R_1, respectively. Considering this, it is concluded that the Q factor amplification leads to increase in $S^{Z_{\rm in}}$, and consequently, expands the sensing and communication range. These features are illustrated in Fig. 16 .

C. Power Consumption Characteristics of Wide-Area Sensing and Communication Functions

Though the Q controllable antenna has positive aspects in widening the effective area of sensing and communication, it also has negative aspects of an additional energy requirement. Thus, it is meaningful to clarify the required power consumption.

In case of sensing and communication functions, the total power injected to the circuit system and the total power consumption is equal, and this total power represents the performance. Thus, injected power that is easily measurable is dealt as representative of power consumption.

An additional experiment to evaluate the power consumption was conducted with basically the same experimental setup and circuit element values. The difference is that the V_{ds} value has been decreased to 1.5 V, which is slightly above the minimum value guaranteeing the FET to be operated in the saturation region. This is due to the fact that the $V_{\rm ds}$ value can be decreased

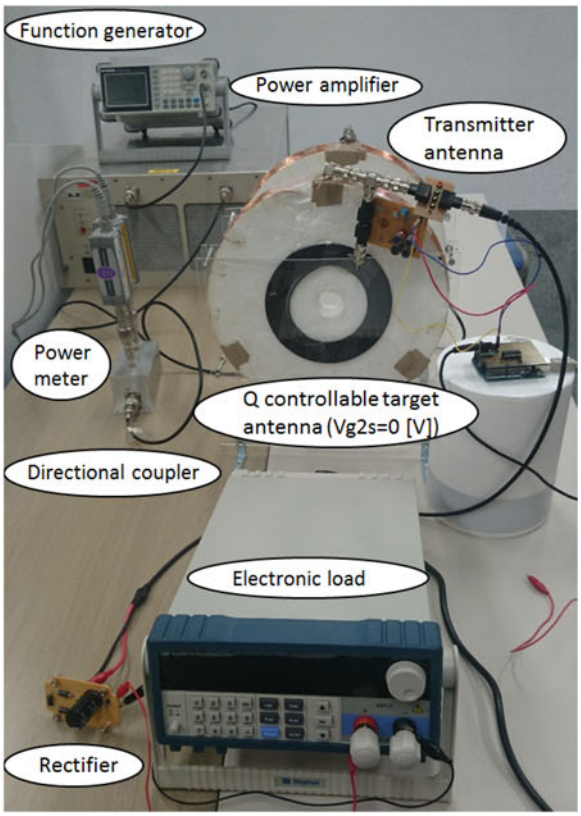

(a)

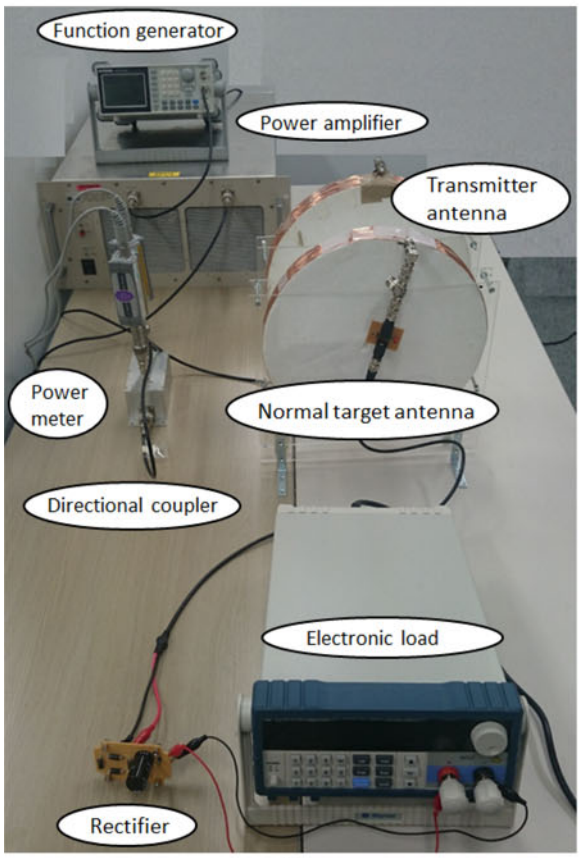

(b)

Fig. 21. Experimental setup of wireless power transmission. (a) Configuration with Q controllable antenna. (b) Normal configuration.

without any deterioration in antenna performance, while the power $P_{\rm ds}$ injected from $V_{\rm ds}$ has quite large proportion.

The experimental result of impedance characteristics of the Q controllable antenna is shown in Fig. 17 . It shows that the Q factor can be amplified to same extent as that of $V_{\rm ds}$=12 V, while the imaginary part of the impedance is suppressed and the resonance is maintained. Thus, it can be said that the reduction of $P_{\rm ds}$ due to lowered $V_{\rm ds}$ is realized without any deterioration in antenna performance. It should be noted that the control voltage V_{g2s} corresponding to each Q factor amplification differs from that of $V_{\rm ds}$=12 V due to the change in the operating point of FET.

The power consumption is discussed regarding Q factor amplification and distance between antennas as variable parameters. The power consumption of the system can be derived as the summation of power injected from $V_{\rm src}$, $V_{\rm ds}$, $V_{\rm bias}$, and V_{g2s} expressed as $P_{\rm src}$, $P_{\rm ds}$, $P_{\rm bias}$, and P_{g2s}, respectively. Here, the maximum power consumption of the system is the indicator of the effectiveness of the proposed method.

In the experiment, the incident power injected into the transmitter antenna is set to -25 dBm, which is the same value with that of the previous experiment. As a result, $I_{\rm bias}$ and I_{g2s} became constant value of 1.131 and 0 mA, independent to Q factor amplification and antenna distance. Therefore, $P_{\rm bias}$ and P_{g2s} showed the constant value of 1.131 mW ($V_{\rm bias}$=1.0 V) and 0 mW. Furthermore, $P_{\rm ds}$ which represents the injected power for Q factor amplification is much higher than $P_{\rm src}$ which represents the original input power to transmitter. Thus, the power consumption of the system is maximized when the $P_{\rm ds}$ shows maximum value. Considering these facts, characteristics of $P_{\rm ds}$ against Q factor amplification and antenna distance are evaluated as follows.

As shown in (32), $P_{\rm ds}$ is calculated as a mean value of instantaneous power $p_{\rm ds}(t)$ over one cycle T [s]. The equation shows that only $I_{b\ ({\rm DC})}$ (dc component of drain current) leads to power consumption

$$\begin{aligned} P_{\rm ds} &= \frac{1}{T}\int_0^T p_{\rm ds}(t)\cdot dt \\ &= \frac{V_{ds}}{T}\int_0^T \left[I_{b\ ({\rm DC})}\cdot dt + I_{b\ ({\rm AC})}\cdot dt\right] \\ &= V_{\rm ds} I_{b\ ({\rm DC})}. \end{aligned} \tag{32}$$

The experimental result of $I_{b\ ({\rm DC})}$ and $I_{b\ ({\rm AC})}$ against antenna distance, where Q amplification factor is fixed to 21.58, is shown in Fig. 18 . Since the FET is operated in saturation region, $I_{b\ ({\rm DC})}$ shows approximately constant value determined by V_{g2s} and $V_{\rm bias}$. Therefore, $P_{\rm ds}$ is also independent to antenna distance. Here, $I_{b\ ({\rm DC})}$ should be larger than $I_{b\ ({\rm AC})}$ (i.e., drain current does not become less than zero) for the FET to guarantee stable performance of voltage-to-current converter (i.e., transconductance), while $I_{b\ ({\rm AC})}$ become maximum in the distance of impedance matching (${\rm Re}(Z_{\rm in(short)}) = Z_0$) as will hereinafter be described in detail at the Appendix. In response, the following discussion show the result at the impedance

TABLE VI
EXPERIMENTAL RESULTS OF WIRELESS POWER TRANSMISSION

Distance [m]	Target Load [Ω]	Input Power [W]	Transmitted Power [W]	Efficiency [%]	Configuration
0.15	75	7.07	5.08	71.9	Q control antenna
0.15	24	8.79	5.14	58.5	Q control antenna
0.3	24	15.43	6.32	41.0	Q control antenna
0.3	24	14.63	6.1	41.7	Normal antenna

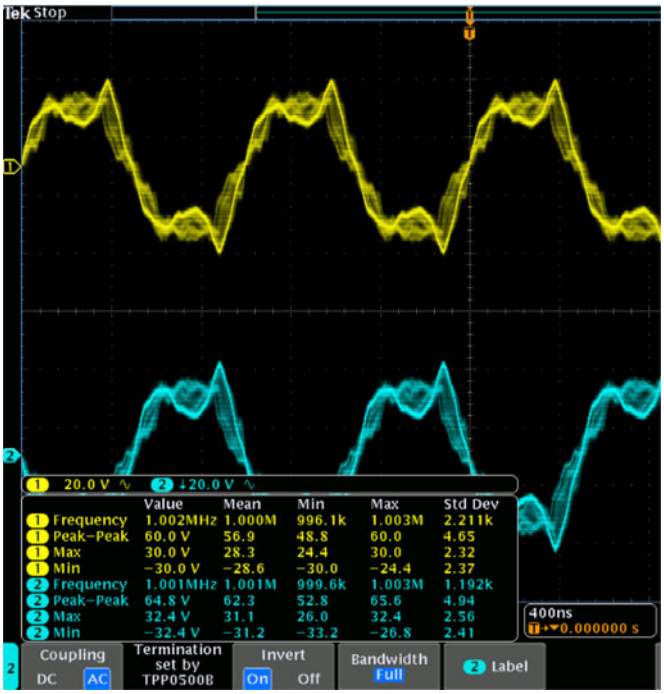

Fig. 22. Voltage waveforms of FET and boost antenna.

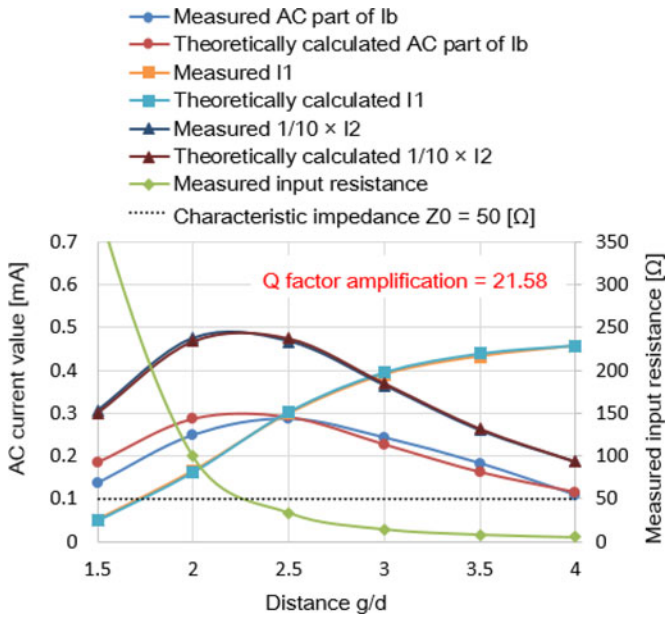

Fig. 23. Measured and theoretically calculated current flow in each antenna, and measured input resistance $\mathrm{Re}(Z_{\mathrm{in(short)}})$ versus normalized antenna distance g/d, in case of Q factor amplification of 21.58 times.

matching distance, in order to also verify whether the condition of $I_{b\ (\mathrm{DC})} > I_{b\ (\mathrm{AC})}$ is satisfied or not.

The experimental result of $I_{b\ (\mathrm{DC})}$ and $I_{b\ (\mathrm{AC})}$ versus Q amplification factor at the impedance matching distance is shown in Fig. 19 . It shows that $I_{b\ (\mathrm{DC})}$ increases with the Q amplification factor and finally saturate to a constant value. This is because the dual-gate FET has the cascode structure of two FETs, and the $I_{b\ (\mathrm{DC})}$ controlled by V_{bias} in the operation at saturation region is also regulated by the V_{g2s}. The regulation is weakened as V_{g2s} becomes larger, and the saturation characteristics finally comes closer to that of single FET which leads in $I_{b\ (\mathrm{DC})}$ to hit a peak at the drain current of the single FET. It should be noted that the transconductance performance is ensured because $I_{b\ (\mathrm{DC})} > I_{b\ (\mathrm{AC})}$ is satisfied in every Q factor amplification value.

Finally, total power consumption and each detailed power consumption verses Q amplification factor at the impedance matching distance is shown in Fig. 20.Here, P_{src} is calculated from (33) by P_{fwd} and measured reflection coefficient Γ

$$P_{\mathrm{src}} = (1 - |\Gamma|^2) P_{\mathrm{fwd}}. \tag{33}$$

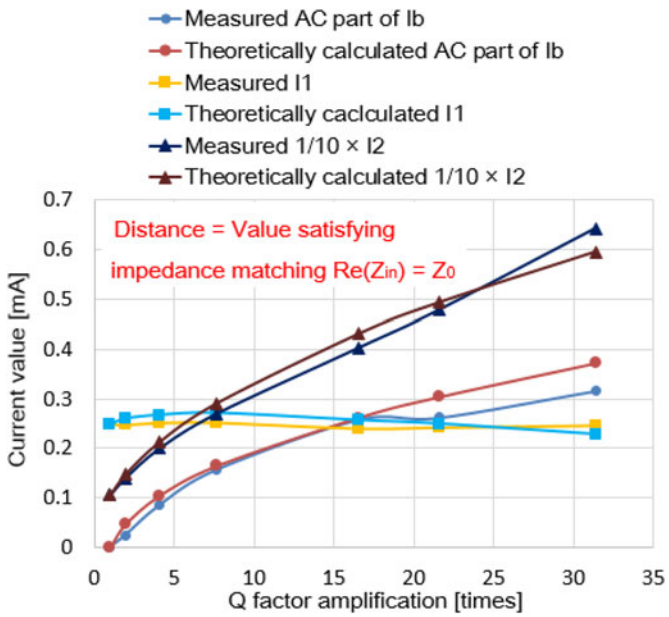

Fig. 24. Measured and theoretically calculated current flow in each antenna versus Q factor amplification, in case of impedance matching distance.

The details show that the $P_{\rm ds}$ and $P_{\rm bias}$, which is the power injected for Q amplification, are much higher than the original $P_{\rm src}$. This confirms that the power consumption has increased in the Q controllable antenna. However, the value of the total power consumption is about 3 mW in maximum, which is comparatively small than common devices commercialized or in research for position sensing and communication as shown in Table V [38]–[44]. Moreover, since the proposed sensing and communication functions are assuming the combination use with wireless charging, the power consumption of several milliwatts will be trivial.

D. Power Transmission Characteristics of Charging Function

As mentioned in Section IV-C, the Q control function is turned OFF in the charging function in order to avoid the meaningless power consumption at the target side.

Considering this, the power transmission experiments have been conducted in case of two configurations: the configuration with Q controllable antenna under condition of Q control function turned OFF (control voltage V_{g2s} is set to 0 V), and the configuration composed of normal antennas. The transmitter and target antennas in both configuration are identical and the design parameters correspond to Table III.

The setup and results are shown in Fig. 21 and Table VI , respectively. Results prove that the transmission efficiency is identical in both cases. Fig. 22 shows the voltage waveforms of FET (upper line) and boost antenna (bottom line). Drain current is $I_b = 0$ A due to $V_{g2s} = 0$ V. However, though the induction voltage from target antenna appears in the boost antenna as shown in Fig. 22, the target antenna does not lose any energy because the electric current does not appear in the boost antenna. This matches the fact that the transmission efficiency is identical in both cases (i.e., does not deteriorate from the case using normal antennas).

VII. Conclusion

The functions such as sensing at the transmitter and wireless communication from the target are known to be the essential elements to realize the standard wireless charging system via coupled magnetic resonances. Due to their hardware compatibility with wireless charging and other additional benefits, passive magnetoquasistatic sensing and ASK-type load modulation are gaining attention as the protocol of sensing and communication functions. However, these protocols have the problem of narrow effective area. Thus, the solution to this problem has been introduced with theoretical details and actual experiments.

First, from the theoretical analysis of effective area in passive magnetoquasistatic sensing and ASK-type load modulation, it is pointed out that the increase of Q factor of the antenna can widen the effective area of both sensing and communication.

Next, the Q controllable antenna which virtually acts as the Q factor is increased was introduced. Then, the wide-area sensing and communication configured by replacing the target antenna with the Q controllable antenna was introduced. Here, the basic mechanisms were explained based on circuit theory.

Finally, the experiment setup of Q controllable antenna itself and the wide-area sensing and communication have been both developed and the basic characteristics were evaluated through experiments. The results showed that the Q factor can be increased until the resonance collapses, and the increase of Q factor has the potential to widen the effective area of sensing and communication, while the additional power consumption is admissible level. The collapse of resonance can be suppressed by decreasing the imaginary part of the antenna impedance as much as possible. Moreover, the power transmission ability does not deteriorate by turning OFF the Q control function during the wireless charging.

Future work will focus on application of the proposed methods to the wireless charging and navigation system for AGVs.

Appendix

The power consumption of the wide-area sensing and communication has been already discussed. Here, current flow in each antenna is discussed. The voltage value can be derived from the current value and circuit element values. These results could be useful for understanding the behavior of the system and selection of the circuit elements in the actual development. The experimental setup and circuit element values are same as that of the experiment conducted in Section VI-C.

The theoretical equations of I_1, I_2, and $I_{b\ (\rm AC)}$ shown in (36)–(38) are derived from (21)–(23), (28), (34), and (35). These equations assume the ideal case of system operating in the purely resonant condition by neglecting the imaginary part of the impedance. α_{mp} representing the Q factor amplification is introduced for simplifying the expressions:

$$I_1 = \sqrt{\frac{(1-\Gamma^2)P_{\rm fwd}}{Z_{\rm in(short)}}} \tag{34}$$

$$\Gamma = \frac{Z_{\rm in(short)} - Z_0}{Z_{\rm in(short)} + Z_0} \tag{35}$$

$$I_1 = \frac{2}{R_1 + Z_0 + \alpha_{mp}\frac{\omega_0^2 L_{12}^2}{R_2}}\sqrt{Z_0}\sqrt{P_{\rm fwd}} \tag{36}$$

$$I_2 = \frac{2\omega_0 L_{12}\alpha_{mp}}{R_2(R_1 + Z_0 + \alpha_{mp}\frac{\omega_0^2 L_{12}^2}{R_2})}\sqrt{Z_0}\sqrt{P_{\rm fwd}} \tag{37}$$

$$I_{b\ (\rm AC)} = \frac{2L_{12}(\alpha_{mp}-1)}{L_{b2}(R_1 + Z_0 + \alpha_{mp}\frac{\omega_0^2 L_{12}^2}{R_2})}\sqrt{Z_0}\sqrt{P_{\rm fwd}} \tag{38}$$

where

$$\alpha_{mp} = \frac{R_2}{R_2 - g_m\omega_0^2 L_{b2} L_2}. \tag{39}$$

Measured and theoretically calculated value of I_1, I_2, $I_{b\ (\rm AC)}$ and measured input resistance $\mathrm{Re}(Z_{\rm in(short)})$ versus antenna distance, at the Q factor amplification $\alpha_{mp} = 21.58$, is shown in Fig. 23. Since the value of I_2 is comparatively large, tenth part of the original value is shown. The measured and theoretically calculated value matches well in each current. I_2 and $I_{b\ (\rm AC)}$ become maximum in same distance where impedance matching

($Re(Z_{\mathrm{in(short)}}) = Z_0$) is satisfied, termed as the impedance matching distance. This can be explained as follows.

Mutual inductance L_{12} in case of the distance maximizing $I_{b\ (\mathrm{AC})}$ (or I_2) is derived as following equation from (38):

$$\frac{\partial I_{b\ (\mathrm{AC})}}{\partial L_{12}} = 0 \quad \Rightarrow \quad \alpha_{mp}\frac{\omega_0^2 L_{12}^2}{R_2} = Z_0 + R_1. \tag{40}$$

Thus, the impedance matching condition expressed as $\mathrm{Re}(Z_{\mathrm{in(short)}}) = Z_0$ is satisfied as follows by the approximation:

$$Z_{\mathrm{in(short)}} = R_1 + \alpha_{mp}\frac{\omega_0^2 L_{12}^2}{R_2} = Z_0 + 2R_1 \simeq Z_0. \tag{41}$$

In order to evaluate the maximum current of the I_2, which is comparatively larger than other currents, the measured and theoretically calculated current versus Q amplification factor at the impedance matching distance is shown in Fig. 24 . The measured and theoretically calculated value matches well in each current. I_1 is approximately constant value, while the I_2 and $I_{b\ (\mathrm{AC})}$ are increasing as the Q factor amplification rises. The maximum current of I_2 showed 6.42 mA at the Q factor amplification $\alpha_{mp} = 31.37$.

REFERENCES

[1] S. C. Tang, "A low-operating-voltage wireless intermediate-range scheme for energy and signal transmission by magnetic coupling for implantable devices," *IEEE J. Emerg. Sel. Topics Power Electron.*, vol. 3, no. 1, pp. 242–251, Mar. 2015.

[2] S. C. Tang and N. J. McDannold, "Power loss analysis and comparison of segmented and unsegmented energy coupling coils for wireless energy transfer," *IEEE J. Emerg. Sel. Topics Power Electron.*, vol. 3, no. 1, pp. 215–225, Mar. 2015.

[3] A. Zaheer, G. A. Covic, and D. Kacprzak, "A bipolar pad in a 10-kHz 300-W distributed IPT system for AGV applications," *IEEE Trans. Ind. Electron.*, vol. 61, no. 7, pp. 3288–3301, Jul. 2014.

[4] T. Sekitani, M. Takamiya, Y. Noguchi, S. Nakano, Y. Kato, T. Sakurai, and T. Someya, "A large-area wireless power-transmission sheet using printed organic transistors and plastic MEMS switches," *Nat. Mater.*, vol. 6, no. 6, pp. 413–417, 2007.

[5] X. Liu and S. Y. R. Hui, "Simulation study and experimental verification of a universal contactless battery charging platform with localized charging features," *IEEE Trans. Power Electron.*, vol. 22, no. 6, pp. 2202–2210, Nov. 2007.

[6] S. Y. R. Hui, "Planar wireless charging technology for portable electronic products and Qi," *Proc. IEEE*, vol. 101, no. 6, pp. 1290–1301, Jun. 2013.

[7] A. Kurs, A. Karalis, R. Moffatt, J. D. Joannopoulos, P. Fisher, and M. Soljacic, "Wireless power transfer via strongly coupled magnetic resonances," *Science*, vol. 317, no. 5834, pp. 83–86, 2007.

[8] B. L. Cannon, J. F. Hoburg, D. D. Stancil, and S. C. Goldstein, "Magnetic resonant coupling as a potential means for wireless power transfer to multiple small receivers," *IEEE Trans. Power Electron.*, vol. 24, no. 7, pp. 1819–1825, Jul. 2009.

[9] A. P. Sample, D. A. Meyer, and J. R. Smith, "Analysis, experimental results, and range adaptation of magnetically coupled resonators for wireless power transfer," *IEEE Trans. Ind. Electron.*, vol. 58, no. 2, pp. 544–554, Feb. 2011.

[10] Y. Zhang, Z. Zhao, and K. Chen, "Frequency decrease analysis of resonant wireless power transfer," *IEEE Trans. Power Electron.*, vol. 29, no. 3, pp. 1058–1063, Mar. 2014.

[11] T. P. Duong and J.-W. Lee, "Experimental results of high-efficiency resonant coupling wireless power transfer using a variable coupling method," *IEEE Microw. Wireless Compon. Lett.*, vol. 21, no. 8, pp. 442–444, Aug. 2011.

[12] S. Nakamura, R. Koma, and H. Hashimoto, "Efficient wireless power transmission based on position sensing using magnetic resonance coupling," *SICE J. Control, Meas. Syst. Integration*, vol. 5, no. 3, pp. 153–161, 2012.

[13] K. M. Farinholt, G. Park, and C. R. Farrar, "RF energy transmission for a low-power wireless impedance sensor node," *IEEE Sens. J.*, vol. 9, no. 7, pp. 793–800, Jul. 2009.

[14] N. Kawashima, K. Takeda, H. Matsuoka, Y. Fujii, and M. Yamamoto, "Laser energy transmission for a wireless energy supply to robots," in *Proc. 22nd Int. Symp. Autom. Robot. Constr.*, 2005, pp. 373–380.

[15] E. Waffenschmidt, "Wireless power for mobile devices," in *Proc. IEEE 33rd Int. Telecommun. Energy Conf.*, 2011, pp. 1–9.

[16] I. Mayordomo, T. Drager, P. Spies, J. Bernhard, and A. Pflaum, "An overview of technical challenges and advances of inductive wireless power transmission," *Proc. IEEE*, vol. 101, no. 6, pp. 1302–1311, Jun. 2013.

[17] P. Manivannan and S. Bharathiraja, "Qi open wireless charging standard—A wireless technology for the future," *Int. J. Eng. Comput. Sci.*, vol. 2, no. 3, pp. 573–579, 2013.

[18] V. Jiwariyavej, T. Imura, and Y. Hori, "Coupling coefficients estimation of wireless power transfer system via magnetic resonance coupling using information from either side of the system," *IEEE J. Emerg. Sel. Topics Power Electron.*, vol. 3, no. 1, pp. 191–200, Mar. 2014.

[19] S. Nakamura and H. Hashimoto, "Error characteristics of passive position sensing via coupled magnetic resonances assuming simultaneous realization with wireless charging," *IEEE Sens. J.*, vol. 15, no. 7, pp. 3675–3686, Jul. 2015.

[20] D. D. Arumugam and D. S. Ricketts, "Passive magnetoquasistatic position measurement using coupled magnetic resonances," *IEEE Antennas Wireless Propag. Lett.*, vol. 12, pp. 539–542, 2013.

[21] L. Catarinucci, S. Tedesco, and L. Tarricone, "Customized ultra high frequency radio frequency identification tags and reader antennas enabling reliable mobile robot navigation," *IEEE Sens. J.*, vol. 13, no. 2, pp. 783–791, Feb. 2013.

[22] V. Viikari, P. Pursula, and K. Jaakkola, "Ranging of UHF RFID tag using stepped frequency read-out," *IEEE Sensors J.*, vol. 10, no. 9, pp. 1535–1539, Sep. 2010.

[23] F. Raab, E. B. Blood, T. O. Steiner, and H. R. Jones, "Magnetic position and orientation tracking system," *IEEE Trans. Aerospace Electron. Syst.*, vol. AES-15, no. 5, pp. 709–717, Sep. 1979.

[24] E. A. Prigge and J . P. How, "Signal architecture for a distributed magnetic local positioning system," *IEEE Sens. J.*, vol. 4, no. 6, pp. 864–873, Dec. 2004.

[25] M. Dionigi, G. de Angelis, A. Moschitta, M. Mongiardo, and P. Carbone, "A simple ranging system based on mutually coupled resonating circuits," *IEEE Trans. Instrum. Meas.*, vol. 63, no. 5, pp. 1215–1223, May 2014.

[26] G. Pirkl, K. Stockinger, K. Kunze, and P. Lukowicz, "Adapting magnetic resonant coupling based relative positioning technology for wearable activity recognition," in *Proc. IEEE Symp. Wearable Comput.*, 2008, pp. 47–54.

[27] C. C. Tsang, P. H. W. Leong, G. Zhang, C. F. Chung, Z. Dong, G. Shi, and W. J. Li, "Handwriting tracking based on coupled μIMU/electromagnetic resonance motion detection," in *Proc. IEEE Int. Conf. Robot. Biomimetics*, 2007, pp. 377–381.

[28] Z. Tang, B. Smith, J. H. Schild, and P. H. Peckham, "Data transmission form an implantable biotelemeter by load-shift keying using circuit configuration modulator," *IEEE Trans. Biomed. Eng.*, vol. 42, no. 5, pp. 524–528, May 1995.

[29] J. Cho, K. W. Min, and S. Kim, "An ASK modulator and antenna driver for 13.56 MHz RFID readers and NFC devices," *IEICE Trans. Commun.*, vol. 89, no. 2, pp. 598–600, Feb. 2006.

[30] A. Bletsas, A. G. Dimitriou, and J. N. Sahalos, "Improving backscatter radio tag efficiency," *IEEE Trans. Microw. Theory Tech.*, vol. 58, no. 6, pp. 1502–1509, Jun. 2010.

[31] S. Y. Lee and H. W. Yang, "Navigation of automated guided vehicles using magnet spot guidance method," *Robot. Comput.-Integr. Manuf.*, vol. 28, no. 3, pp. 425–436, 2012.

[32] S. Kamewaka and S. Uemura, "A magnetic guidance method for automated guided vehicle," *IEEE Trans. Magn.*, vol. MAG-23, no. 5, pp. 2416–2418, Sep. 1987.

[33] E. Freund and F. Dierks, "Laser scanner based free navigation of autonomous vehicle," *Control Eng. Practice*, vol. 2, no. 2, pp. 299–304, 1994.

[34] S. Sabikan, M. Sulaiman, S. N. S. Salim, and M. F. Miskon, "Vision based automated guided vehicle for navigation and obstacle avoidance," in *Proc. 2nd Int. Conf. Eng. ICT*, 2010, pp. 18–20.

[35] Agilent Technologies. (2015, Jul.). *Impedance Measurement Handbook*. [Online]. Available: http://cp.literature.agilent.com/litweb/pdf/5950-3000.pdf

[36] Agilent Technology. (2015, Jul.). *ENA-L RF Network Analyzers E5061A and E5062A Data Sheet*. [Online]. Available: http://cp.literature.agilent.com/litweb/pdf/5989-0018EN.pdf
[37] W. H. Hayt, *Engineering Electromagnetics*. New York, NY, USA: McGraw-Hill, 1989.
[38] (2015, Jul.). [Online]. Available: http://www.hokuyo-aut.jp/02sensor/07scanner/download/pdf/UBG-04LX-F01_spec1.pdf
[39] J. Seitz, T. Vaupel, and J. Thielecke, "Wi-Fi azimuth and position tracking:Signal propagation, modeling and evaluation," in *Proc. IEEE 16th Int. Conf. Inf. Fusion*, 2013, pp. 1479–1486.
[40] X. Zhang, R. Shrestha, and K. Wahid, "An efficient algorithm for localization using RSSI based on ZigBee," in *Proc. IEEE 28th Can. Conf. Elect. Comput. Eng.*, 2015, pp. 366–369.
[41] (2015, Jul.). [Online]. Available: http://www.decawave.com/sites/default/files/product-pdf/dwm1000-product-brief.pdf
[42] M. E. Rida, F. Liu, Y. Jadi, A. A. A. Algawhari, and A. Askourih, "Indoor location position based on Bluetooth Signal Strength," in *Proc. IEEE 2nd Int. Conf. Inf. Sci. Control Eng.*, 2015, pp. 769–773.
[43] S. S. Samer and S. N. Zahi, "A standalone RFID indoor positioning system using passive tags," *IEEE Trans. Ind. Electron.*, vol. 58, no. 5, pp. 1961–1970, 2011.
[44] (2015, Jul.). [Online]. Available: http://polhemus.com/_assets/img/FASTRAK_Brochure.pdf

Sousuke Nakamura (M'12) received the B.E., M.E., and Dr. Eng. degrees in electrical engineering from the University of Tokyo, Tokyo, Japan, in 2005, 2007, and 2012, respectively.

He joined the Chuo University, Tokyo, as an Assistant Professor in 2012. His current research interests include wireless charging system for mobile devices.

Dr. Nakamura is a Member of the Society of Instrument and Control Engineers of Japan, the Institute of Electrical Engineers of Japan, and the Robotics Society of Japan.

Masato Namiki (S'13) received the B.E. degree in electrical, electronic, and communication engineering from the Chuo University, Tokyo, Japan, in 2014, where he is currently working toward the M.E. degree.

His current research interests include performance enhancement of wireless charging system.

Yasuhiro Sugimoto (SM'06) received the B.E. degree from the Tokyo Institute of Technology, Tokyo, Japan, the M.E. degree from the University of Michigan, Ann Arbor, MI, USA, and the Doctor of Engineering degree from the Tokyo Institute of Technology in 1973, 1980, and 1991, respectively.

He joined Toshiba Semiconductor Group in 1973 and involved in the development of analog VLSIs. Since 1992, he has been with the Faculty of Science and Engineering, Chuo University, Tokyo, where he is currently a Professor in the Department of Electrical, Electronic, and Communication Engineering. He is the author of seven books. His main research interests include the design and development of new circuits in mixed-signal and RF LSIs.

Dr. Sugimoto received the 1989 Best Papers Award of European Solid-State Circuits Conference and the 1998 IEICE Best Papers Award. He is a Fellow of the Institute of Electronics, Information and Communication Engineers of Japan and a Member of the Japan Consulting Engineers Association.

Hideki Hashimoto (S'83–M'84–SM'04–F'06) received the B.E., M.E., and Dr.Eng. degrees in electrical engineering from the University of Tokyo, Tokyo, Japan, in 1981, 1984, and 1987, respectively.

He joined the Institute of Industrial Science, University of Tokyo, as a Lecturer in 1987, and was an Associate Professor from 1990 to 2010. He moved to Chuo University, Tokyo, as a Professor in 2011. From 1989 to 1990, he was a Visiting Researcher at the Massachusetts Institute of Technology, Cambridge, MA, USA. His research interests include the control and robotics fields, in particular, intelligent systems.

Dr. Hashimoto was the Vice-President of the IEEE Industrial Electronics Society (IES) and the Intelligent Transportation Systems Council (ITSC), and a Board Member of the Society of Instrument and Control Engineers of Japan. He initiated the IEEE/ASME International Conference on Advanced Intelligent Mechatronics in 1997. He is a Member of the IEEE IES, the IEEE Robotics and Automation Society, ITSC, the Institute of Electrical Engineers of Japan, and the Robotics Society of Japan.